VERIFICATION OF THE USE OF MICRO-CT SCANNING TO ASSESS THE FEATURES OF ENTIRE SQUAT TYPE DEFECTS

Shaun Earl [1,*], Kathryn E. Rankin[2], Roger Lewis [3], Lindsey Smith [4], W. Mark Rainforth [1]

[1] Department of Material Science and Engineering, Sir Robert Hadfield Building, Mappin Street, The University of Sheffield, S1 3JD, UK

[2] µ-VIS X-ray Imaging Centre, Faculty of Engineering and Physical Sciences, The University of Southampton, SO17 1BJ

[3] Department of Mechanical Engineering, Sir Frederick Mappin Building, Mappin Street, The University of Sheffield, S1 3JD, UK

[4] Rail Technologies, British Steel, Scunthorpe, UK

[*] E-mail: sjearl1@sheffield.ac.uk

Keywords: Squats; Studs; Rolling Contact Fatigue; microstructural analysis; surface defects; X-ray micro-computed tomography scanning.

Abstract

Squats and studs are defects in railheads that share features, but have different causes. This paper examined four squat and stud samples from three different traffic environments to compare features using µ-CT X-ray scans, surface and subsurface inspection. µ-CT scanning has been used before as a non-destructive method to investigate rail defects, but not the entire defect. The scans were verified and allowed the identification of areas of interest when sectioning the samples further. The scan volumes were also used to create 3D models of the crack networks for the 3 samples that were scanned. All defects contain similar superficial features but the depth and severity of the subsurface damage varies.

This work provides a visualisation of the 3D nature of studs in a way not seen before, as a 3D model the crack network from an in-service defect. The models of two of the defects showed the influence of hollow wheels initiating defects, as the crack seemed to initiate on the field side, grow down and towards the gauge side, before resurfacing as the longitudinal crack noted in all four defect samples. One sample is believed to have initiated due to contamination of the weld and the only squat sample, which failed in track, was believed to be ingot cast steel containing many inclusions.

Three samples were studs and one was a squat. Each defect developed for different reasons, although the two metro samples were similar. One of the studs shows branching of cracks that, based on its changing angle of growth, could continue to grow into transverse defects, breaking the rail. The three defects that were scanned would all be classed as studs, but their crack morphology varies, possibly because they are all from different traffic environments. They also show slight differences to other studs in literature.

1. Introduction

A great deal of research has been conducted in the area of squats, as they cause the need for expensive rail replacement by railway operators [1]–[3]. In the UK, between 4,000 and 10,000 new squats are detected in railway lines every year [4]. Despite growing knowledge in this area, the causes for the initiation of the squats and the reasons for some of the defects to develop transversely (causing the crack to travel down into the rail eventually breaking the railhead) are still unclear. Squats, also known as taches noirs (black spots) and shells, are a defect found on the running surface of the railhead. Squats have some typical features such as the black spots on the running surface and the v-shaped crack that branches towards the gauge corner (Figure 1), but they can vary due to extensive variation in traffic and layout conditions that a rail can experience. They typically comprise of a combination of plastic deformation and a subsurface crack network that may break the surface. Squats usually result in shelling of the upper surface of the rail, but in some situations, the cracks can develop into a transverse defect, leading to a rail break.

Studs are a squat type defect that develop faster than squats [5]. They are caused by sudden heat flux in the running band due to excessive slip, i.e. wheel spin or wheel lock. While they develop faster than squats, they are not believed to break rails like squats can. They do not require plastic deformation of the surface material to form, are not linked with lubricant assisted crack growth [6], do not have the plastic deformation seen in squats and form in the running band rather than towards the gauge corner [5].

Studs arise from high slip leading to thermal damage of the rail. The thermal damage causes residual stress to become locked into the rail surface. There are two residual stress build-up mechanisms; from the temporary expansion and then contraction of the steel due to thermal input and then because of the lattice structure change from pearlitic base-centred cubic (BCC) through austenitic face-centred cubic (FCC) then cooling into martensitic base-centred tetragonal (BCT),
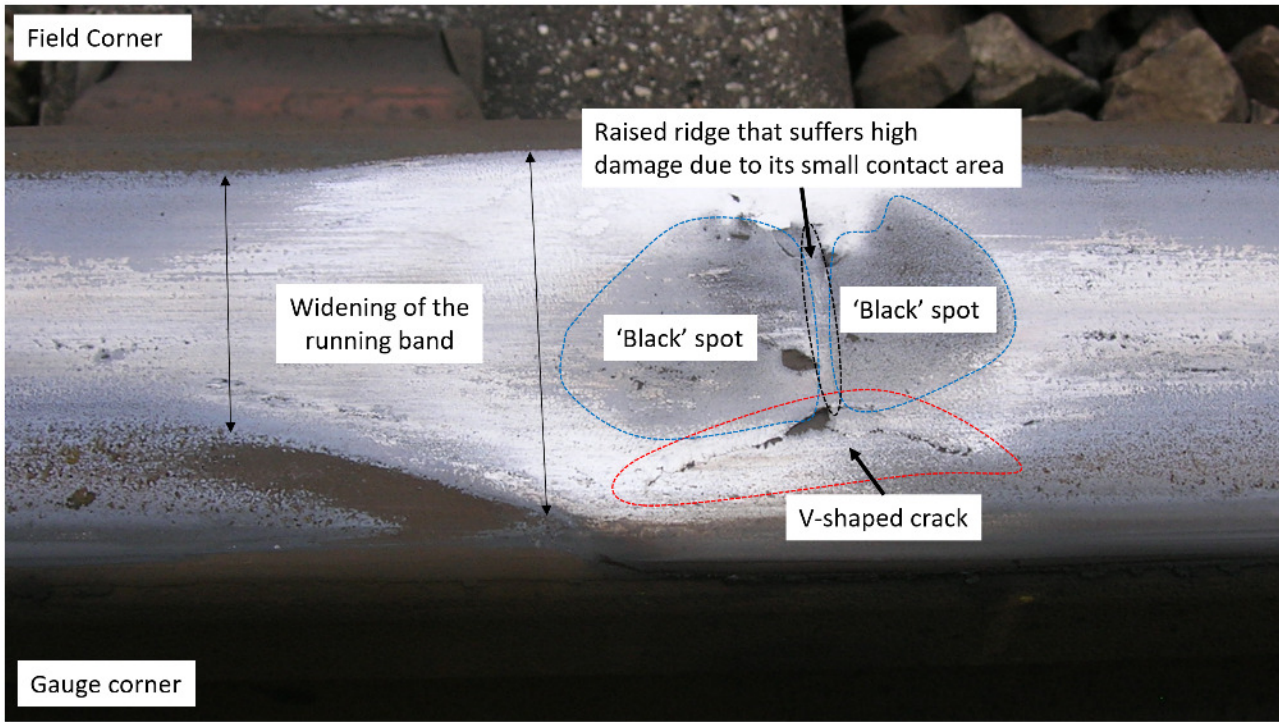
Raised ridge that suffers high
damage due to its small contact area

Widening of the
running band

'Black' spot

'Black' spot

V-shaped crack

Gauge corner

Figure 1: An example of a squat defect. Original image courtesy of British Steel.

which has a different volume to pearlite [7]. A tensile residual stress within the defect would pull cracks open, increasing the stress intensity factor at the crack tip. This results in a crack structure that ultrasonically looks similar to squats, but there are marked differences in their development as summarised by Grassie et al. [5].

Work carried out in Australia on squats refers to running band squats and gauge corner squats, so it could be that the running band squats were indeed studs, considering they are remarked as "often mistaken for wheelburn defects" [8].

These running band or rail crown squats are considered to be similar in nature, but not in degree to wheelburns, are associated with a thick "White Etching Layer" (WEL) and can appear as multiple defects over a short distance [9].

Studs and squats share a similar subsurface crack network once the defect develops and they both have an association with WEL. Only a few samples have been presented as studs [5], so further comparisons between squats and studs would be beneficial to enhance the understanding as to what constitutes a stud and what should be identified as a squat.

The microstructural analysis and comparison of different squat samples should; give clues as to how they initiate, identify differences in any WEL present, show how the different traffic environments affect crack development and provide insight as to why some defects develop into transverse defects whilst others do not. In conjunction with traditional sample preparation techniques, this work utilises the use of X-ray micro-computed tomography (μ-CT) scanning as a non-destructive volumetric inspection tool [10]. This allows accurate targeting of regions of interest within the defect for closer inspection prior to any destructive sample preparations. μ-CT scanning has been used previously to successfully investigate the form of squats by Naeimi et al. [11], who also gives good justifications for why CT scanning is a powerful NDT tool that maximises the information that can be retrieved from a sample. This work builds on this by expanding the scan to the entire defect, which required a 450kV μ-CT scanner.

2. Rail Samples

The samples were sourced from metro, mainline and high speed track in the UK and France. The samples have been characterised using 3D microscope mapping, X-ray μ-CT, optical imaging and scanning electron microscopy (SEM) in order to provide a comparison between them. The characterisation techniques also allow the identification of any samples that are squat type unidentified defects (studs). As a simple comparison, studs do not have the heavily deformed layer on the surface like squats do. Squats take much longer to form than studs: ~100MGTs of traffic to ultrasonic detection as opposed to ~30MGTs for a stud [5]. The samples analysed are shown in Table 1:

Sample number	Location removed from	Traffic type	Grade
1	France	Metro	R260
2	UK	Metro	R220
3	France	Mixed	R260
4	UK	High speed	R260

Table 1: List of samples examined

The samples were subjected to a variety of tests to assess and capture the characteristics of the defect. The tests are shown in Figure 2, although not all samples went through every stage. Surface analysis was carried out to document the surface of the sample and choose points of interest on the sample. It was also used to compare the surface of the samples to each other. μ-CT scanning was not conducted on sample 3 as the surface had already shelled. All samples were sectioned, prepared and analysed optically with the most interesting regions being inspected using SEM.
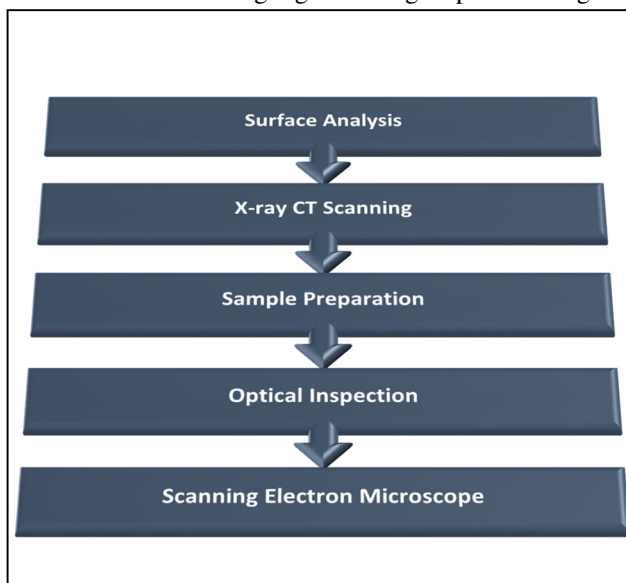

Figure 2: *The sequence of tests conducted on the squat samples*

2.1. Sample 1

Not much is known about the track location and traffic experienced by sample 1 other than it was from an inclined track near a station on a metro line. Sample 1 is shown in Figure 3a. It shows signs of sliding surface damage and the dark spots are quite well developed. It contains a lot of surface damage including four obvious surface cracks, streaks of what is assumed to be white etching layer (WEL), a pit in one of the cracks, what seems to be 'snakeskin' damage just outside the widened running band. WEL is shown in results. 'Snakeskin' is also known as running surface checking or flaking and is a precursor to spalling of the rail surface [12]. There is also the very common V-shaped crack that squats are known to exhibit, although the angle within the V in this crack is more obtuse than expected. There is also a faint series of small cracks along a ridge that extends from the apex of the V-shaped crack out between the two lobes which is often observed as squats develop [13]. On initial inspection, the presence of some lipping on the gauge corner of the sample combined with the typical black spots and v-shaped cracks, made this sample appear to be a squat. The features that makes it more likely to be a stud are; the lack of any significant WEL on the surface of the rail and the minimal plastic deformation. The only plastic deformation found was in the vicinity of cracks and the decarburised lip on the gauge corner. The decarburised lip suggests strong gauge corner contact during sliding conditions and so the inclined track may have also contained a curve.

2.2. Sample 2

This sample was taken from the high rail of a uni-directional rail in a gentle curve just over 1km along a 3.2km distance between two stations. This track has relatively high line speeds and is very busy regarding passenger trains compared to other lines on the same network. However, this sample came from a fairly rural overground section near the end of the line so the train volume may be less.

Sample 2 is shown in Figure 3b, and is post MPI (magnetic particle inspection): a non-destructive test that uses magnetic ink on a white contrasting background to highlight defects in the surface. The long crack seen on the left of Figure 3b, seems to be a combination of the long cracks found at the edge of the running band in samples 1 and 4 (Figure 3a and d respectively) and the expected V-shaped crack typically seen in a classic squat. The crack also has sharp edges unlike the embedded cracks found on the other samples, possibly a sign that the crack is very recent. Sample 2 also has significant discreet material removal. These look like corrosion pits, but are more likely localised delamination and flaking characteristic of "ratchetting" [14]. Ratchetting is incremental plastic deformation of the upper surface of the rail material due to cyclic strain build-up. Unique features in sample 2 are possibly because of traction control being used by the rolling stock on this line. Traction control has been linked to squat development, or more specifically, thermal damage of the rail [15]. With just under 11MGT of traffic, initial thoughts were that it is very likely a stud rather than a squat. Studs are detectable from ~10MGT whereas squats are detectable from ~40MGT, the surface is also smooth to touch unlike squats, which are rough to touch in one direction due to the accumulated strain [5]. There was also no noticeable corrugation on the 1m section of rail, which would add to the dynamic loading and is often found in the vicinity of squats. However, the V-shaped crack can be made out and there is a crack along where the ridge should be.
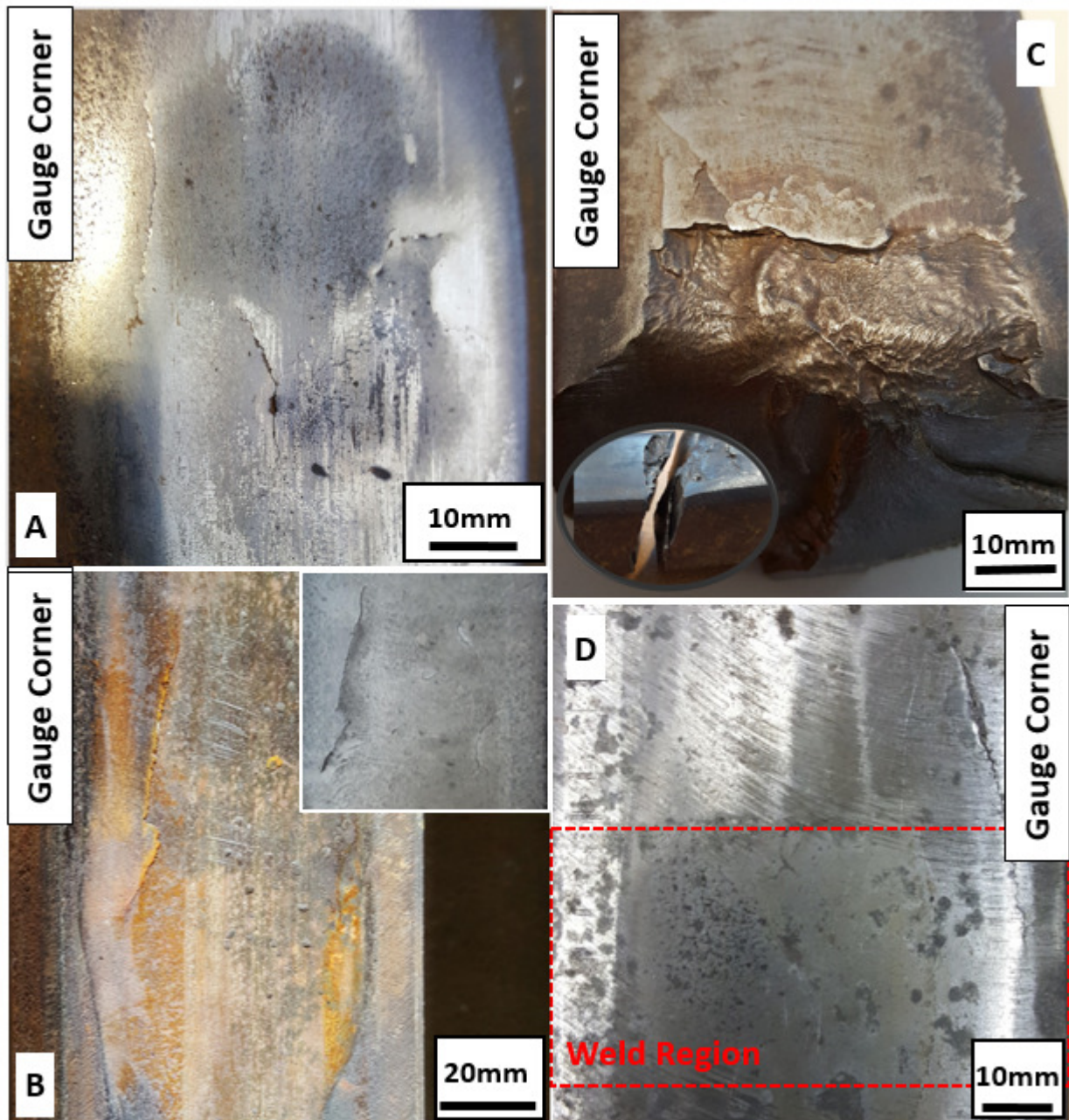
Figure 3: Images of the samples, all of which are a full rail width (~75mm wide) a) Sample 1 b) Sample 2 with magnetic particle inspection image inset to show apex cracks on field side c) Sample 3 with the other half of the defect inset d) Sample 4 with the weld region highlighted

2.3. Sample 3

Sample 3 is a broken rail of unknown MGT, which failed due to a transverse defect, within a squat defect, shown in Figure 3c. Most of the squat was damaged in the break, removing any surface evidence of the expected V-shaped crack. There was not much information to be gained from the shelled lobe either. However, the unbroken lobe of the squat was still available to view. The second lobe was very close to shelling and so presented the opportunity to remove the almost separated plate of surface material from the top of the defect. This allows the inspection of the crack plane below the squat. This plane was covered in oxide but the presence of water may have come from the cutting process due to the coolant flooding the sample. The plane was dry ice blasted to remove the oxide. The plastic flow shown by the folded material right next to the shelled section makes this most likely to be a squat.

2.4. Sample 4

Sample 4, shown in Figure 3d, was initially identified as a squat on an alumina-thermic weld and following an ultrasound test, was believed to be a combination of a squat interacting with a weld defect. The longitudinal crack that runs along the edge of the sample shows that the squat is slightly elongated, possibly linked to the higher train speeds [16]. The lack of deformation in the squat and the traffic total of ~28MGT makes it likely that this is in fact a stud, although a study has shown that 17% of squats are found at welds [17].

147 As with samples 1 and 2, sample 4 has a large crack on the gauge corner side, but not the v-shaped crack that is usually
148 expected of a squat. The sample showed extensive grinding marks across the surface, not including the depressed region
149 of the defect, which was in the weld region. Grinding marks were more extensive than the other samples but this could
150 simply be because grinding had occurred more recently. Grinding marks and other features that increase the roughness of
151 a surface, such as crack mouths and the pits seen in sample 2, can increase the subsurface stress by a factor of eight
152 compared to smooth surface contact [18].

3. Analytical techniques

3.1. Alicona Infinite Focus SL 3D Microscope

156 The infinite focus (IF) microscope is capable of capturing both the form and the roughness of surfaces. It uses a reference
157 point and coordinate system that maps a surface area and can measure surfaces up to 87°, so some features cannot be
158 captured and appear as white regions within the bulk image (areas of no data). The microscope was used with IF-
159 MeasureSuite Version 5.1 software.
160 In order to create the images in this work, two points needed to be specified in the volume of interest. These points had
161 to contain the lowest x, y and z value and the highest x, y, and z value that the volume of interest occupied. By specifying
162 'two corners' of the volume the system then breaks the volume into a 3D grid and takes multiple images at various focal
163 lengths across the entire x-y plane. The software then identifies the regions in each image that are in focus, and knowing
164 these focused positions, stitches them together to provide a 3D model of the surface that can be manipulated by the user.

3.2. X-ray Micro-Computed Tomography (µ-CT) Scanning

167 Micro-focus cone beam X-ray CT (µ-CT) is a non-destructive volumetric imaging method, which works by acquiring a
168 series (thousands) of 2D projection radiograph images based on X-ray photon absorption, as the specimen is rotated
169 around a single axis, usually through 360º. The 2D projection images are then reconstructed into a 3D volumetric dataset
170 using mathematical tomographic reconstruction algorithms, commonly based upon Filtered Back Projection (FBP)[10].
171 The voxel intensity (grey scale value) in the reconstructed volume slice images, reflects a combined function of the
172 variation in X-ray absorption, (which is a function of the specimen's physical and radio-density), and CT artefacts from
173 the acquisition and reconstruction process[10], [19]. Therefore it can be inferred for the reconstructed images in this work,
174 that the brighter voxels represent the dense metallic material, and the darker pixels represent less dense materials, i.e. air,
175 cracks or voids in the sample. Care must be taken when interpreting images as artefacts can provide distorted images [19].

3.3. Data analysis

178 Avizo 9.3 (FEI SAS, Thermo Fisher Scientific, USA) is a 3D materials characterisation software that allows the
179 visualisation and analysis of large data sets. The user can segment volume data to form colour coded models, i.e. grey
180 scale voxels, are labelled with colours corresponding to different structures identified within the specimen, such as
181 different materials and features such as cracks and pores.
182 For this work Avizo was primarily used to map out the planar crack network of the defects within the rail samples. In the
183 orthoslices of the scan the image was changed from greyscale to green and black to make the cracks more visible by eye.
184 A touch screen pad and stylus connected to the computer were used to manually draw in the cracks for each 2D slide,
185 first longitudinally then cross sectional. The model is then improved from a mesh structure into a smoother planar structure
186 using linear interpolation between two known points. The two known points are the lines that have been drawn into the
187 orthoslice. VGStudio MAX (Volume Graphics GmbH, Germany) is a voxel based software that was used to view the
188 orthoslices and take measurements of features within the µ-CT volume data. Fiji/ImageJ is an open source image
189 processing software (National Institutes for Health, USA).

3.4. Microscopy

192 Before micro-preparation, the large rail samples were cut using industrial band saws. Sample 1 is an exception as it was
193 received already cut to approximately 80x100x20mm. Micro-preparation involved the processing of the relatively large
194 rail samples from the size of the defect down to etched and polished samples that would show the pearlitic microstructure
195 under a microscope.
196 The samples were cut using an abrasive disc cutter, mounted in 32mm Bakelite discs, ground and polished down to a 1
197 micron diamond suspension finish. The samples were then etched in 2% nital (2% nitric acid and 98% ethanol) as is
198 typical for steel: this reveals the microstructure. Once revealed the microstructure was inspected and documented using a
199 Nikon Eclipse LV150 optical microscope with Buehler Omnimet software and Zeiss Axio Imager.A2m optical
200 microscope with AxioVision4 software.

3.5. Scanning Electron Microscope (SEM)

203 Images were obtained using an Inspect F Scanning Electron Microscope by FEI company. Samples were prepared in the
204 same way as detailed in 3.3 except they were mounted in conductive bakelite to allow discharge from the sample during
205 SEM use. A beam voltage of 20kV and a spot size of 2.5 were used to capture secondary electron (SE) images.

4. Methodology

4.1. Surface analysis

The surface was mapped from optical images of the samples and using the IF microscope. Attention was focused around surface breaking cracks and vertical irregularities such as grinding marks and pits. The region of interest was identified by specifying a 3D volume and the number of scanned points were reduced by using the 'decimate' function until the file size was manageable (the software gave a warning if it was too large). The 'decimate' function was always used once, twice for relatively large areas but never three times.

4.2. CT scans

The CT scans were conducted on samples 1, 2 and 4 at the µ-VIS X-ray Imaging Centre (University of Southampton, UK) using a custom built, dual source 225/450 kV walk in room (Nikon Metrology, UK). The scans were acquired using a micro-focus 450kV source fitted with a tungsten reflection target together with a Perkin Elmer XRD 1621 CN03 HS detector.

The samples were made as small as possible without cutting into the defect. The smaller the sample could be made, the better the images could be. The sizes of the samples varied slightly depending on the size of the discernible defect. Sample 4 was reduced in size slightly after an initial quick scan allowed a more accurate idea of where the crack network was to be found. At its full size, sample 4 was approximately 8 cm wide, 10.5cm long and 3cm deep and the scan was able to identify the crack network clearly enough to trim the sample. The final size of the samples scanned are shown in Table 2.

Sample	Width (mm)	Length (mm)	Depth (mm)
1	70	55	15
2	74	85	15
4	66	65	26

Table 2: Dimensions of samples that were µ-CT scanned

The width was taken along the bottom of the sample rather than over the curved surface.

Each sample was mounted within a 3mm thick Perspex tube in a vertical orientation, so as to minimise X-ray photon penetration path length. The source to object distance was set to 235 mm, and the source to detector distance was set to 800 mm, achieving a reconstructed voxel (cubic pixel) resolution of 50 µm. 4 mm of copper pre-filtration was used in addition to the aluminium window that forms part of the target housing on the X-ray gun. Each µ-CT scan was performed at 400 kVp (peak voltage) and 248 µA, using a 177ms image exposure time; 2801, 3142 and 2601 projection images were acquired during a full 360º rotation, with 32, 16 and 32 frames averaged per projection, for samples 1, 2 and 4, respectively. The projection images were reconstructed into 2000x2000x2000 voxel 32 bit volumes using the FBP algorithms implemented within X-TEK CTPro 3D and CTAgent software packages (Nikon Metrology, UK).

Two scans were used to cover the full height of sample 2, and the reconstructed volumes were concatenated using Fiji/ImageJ. Each sample's volume was converted to 8 bit in Fiji/ImageJ to reduce the computation time for analysis, and saved as a raw volume for review in VGStudio MAX. The results were viewed as three windows of orthogonal slices through the rail, providing a longitudinal, cross section and aerial view of the rail in orthoslices. The data was also investigated using Avizo, mentioned in section 4.3, building a 3D crack model. Cracks were highlighted every five orthoslices and added to the model, then the planar interpolation feature was used to interpret where the crack was most likely to be between the five slices. The built in crack detection software struggled to identify the cracks accurately if at all, hence the manual segmentation method. This was done for both the longitudinal and cross sectional slices.

4.3 Scan verification

The presence of CT artefacts in the volume images, from effects within the scanning and reconstruction process such as photon scatter, partial volume effect, image noise and beam hardening, could lead to spurious features within the reconstructed volume. A visible artefact when viewing some slides is the apparent 'shadows' that cracks can cast when they get very close to each other (streaking artefacts), this can make it look like there is a small void in the material. In order to be sure that what the scan shows is real it needed to be compared to micrographs of the scanned segment. Shadows that occur along a crack in were of particular interest as they may hold clues as to why the crack plane develops in certain directions.

Measurements were taken using the VGStudio Max software caliper tool and then the sample was marked up with cutting lines in preparation for physically cutting the sample to expose some of the interesting features found in the scans. The samples were prepared as described in section 3.3 and then compared to the slices to see how accurate the scans were.

5. Results

5.1. Sample 1

On sample 1 there were quite a few differences in surface finish, such as the shiny running surface next to the dark corroded region of the black spots, as well as the cracked 'snakeskin' region. There are four obvious cracks on the surface that are identified in: Figure 4 and the scanned images of them are in Figure 5. The longitudinal and obtuse V-shaped crack are found in the other samples, but the L-shaped and Y-shaped cracks are not (shown in Figure 4). The Y-shaped crack has been seen before in a squat sample reported on previously by Tata Steel [20] along with the 'snakeskin' surface damage (see Figure 6). In the Tata Steel report the snakeskin was also found on an area of the rail that did not contain a squat. The dark spot within the V-shaped crack is believed to be a spalled piece of snakeskin as the snakeskin can be faintly seen close to the crack (Figure 5c).
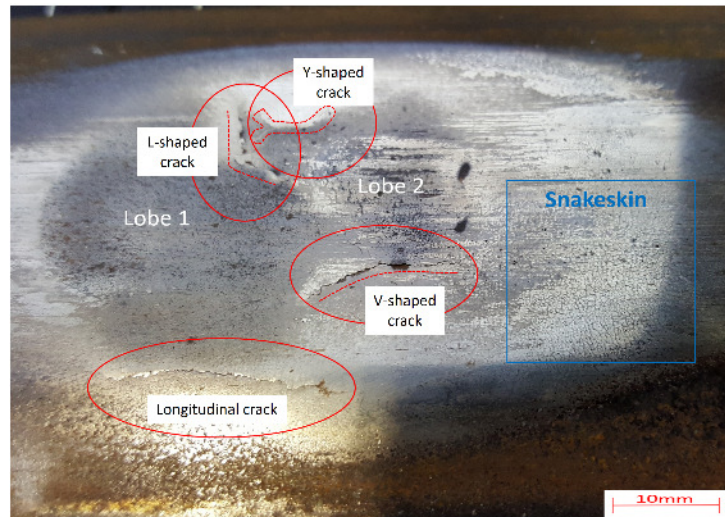

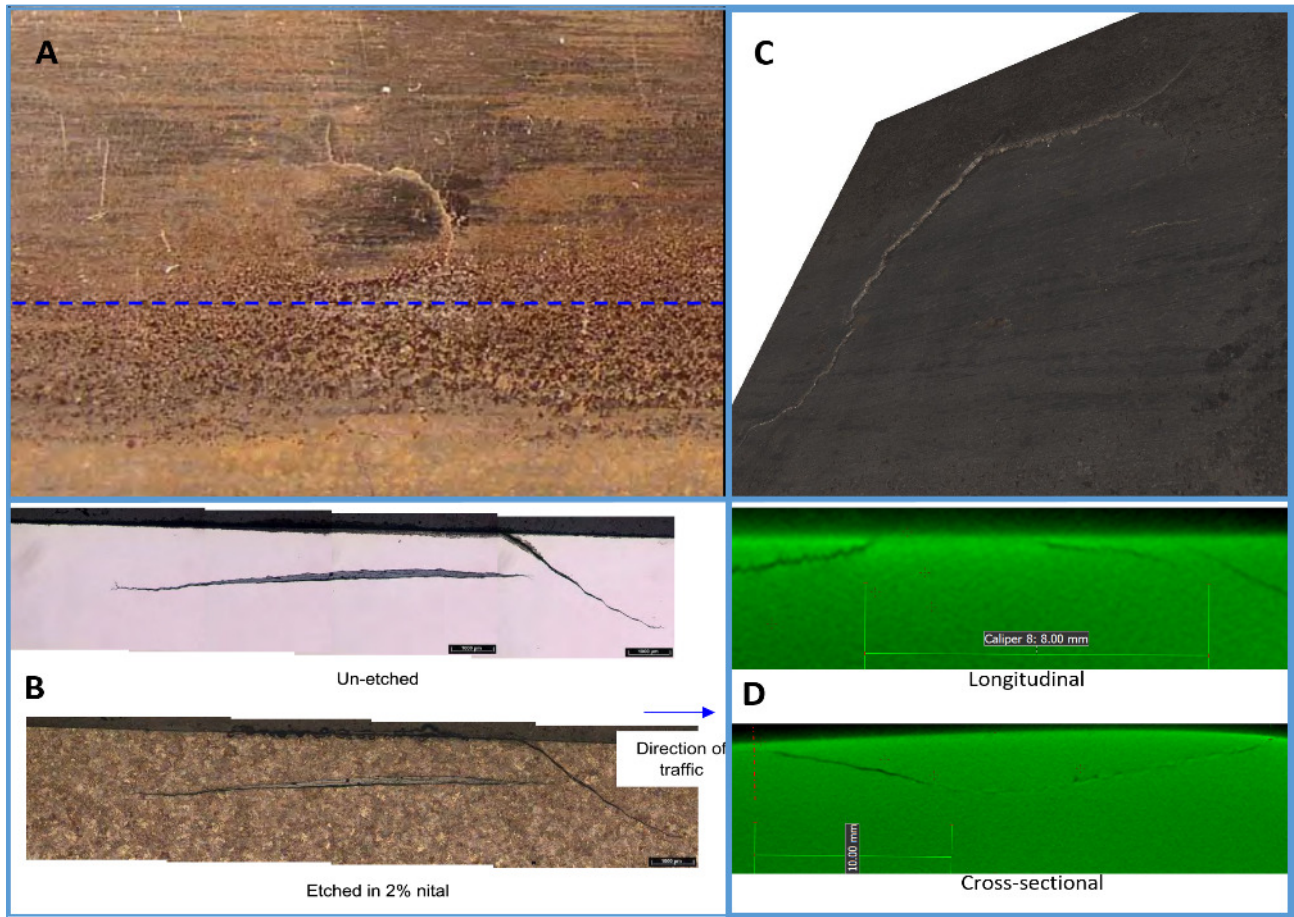*Figure 4: Sample 1 with the cracks marked in red and the snakeskin marked in blue*

Figure 5: Some of the surface features imaged from sample 1 a) The L-shaped crack with 'islands' that appear pink in the scan b) The V-shaped crack with a pit that penetrates into the substructure c) 'Snakeskin' microcracks across the surface of the rail just beyond the defect d) A colour coded overview showing where the images are taken from
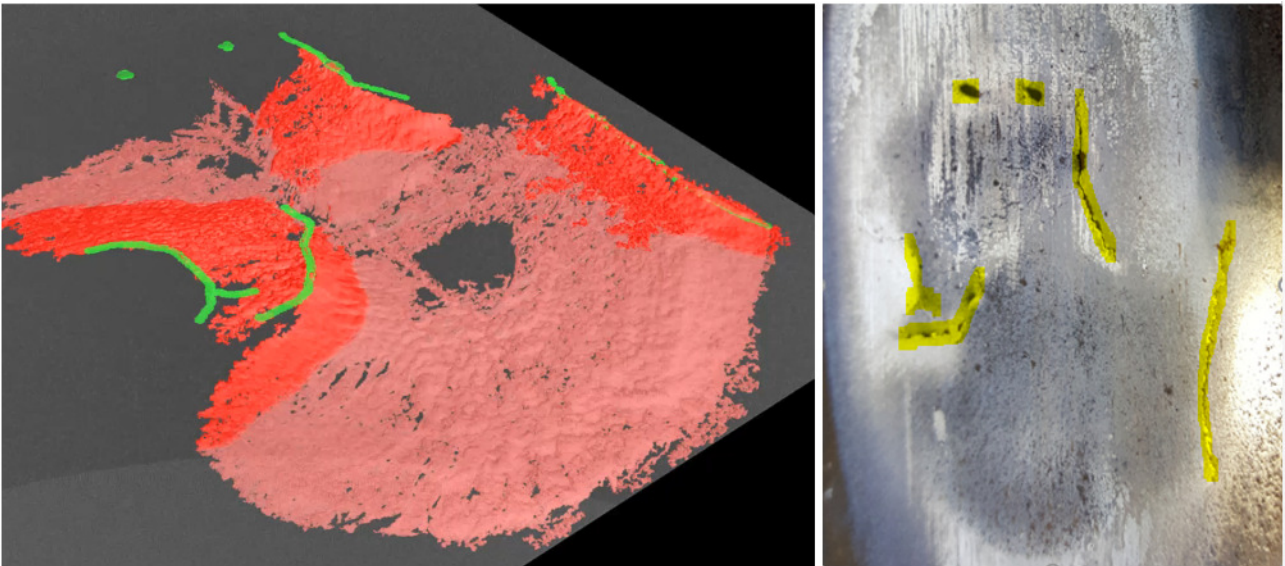
268
269 Figure 6 shows the Y-shaped cracks in sample 1 and the Tata Steel report as surface and subsurface defects. As the Y-
270 shaped crack was the only surface crack in the Tata Steel report it can be assumed that this crack forms first. The shallow
271 depth of the defect in the report compared to sample 1 also suggests that sample 1 is much more developed. Both samples
272 are believed to be from the same metro network. The presence of the two cracks suggests the possibility of one crack
273 initiating subsurface whilst the other initiated on the surface. Using the x-ray scanned volume that Figure 6d was taken
274 from, it can be seen that moving through the sample towards the field corner shows that the cracks stay separate, although
275 they may have connected within the region that was worn away. Moving through the sample towards the gauge corner
276 shows the two cracks connecting as a very shallow crack parallel to the surface that makes up the bottom portion of the
277 Y shape (when viewing the Y as written here).

Figure 6: Comparison of features of a squat from a Tata Steel report [20] with scan results from sample 1. a) The surface of the squat from the report, b) Longitudinal cross sections from the report, c) Surface scan from Alicona of sample 1, d) Longitudinal and cross sectional x-ray scans of sample 1 (red dotted line shows where orthogonal slices cross)
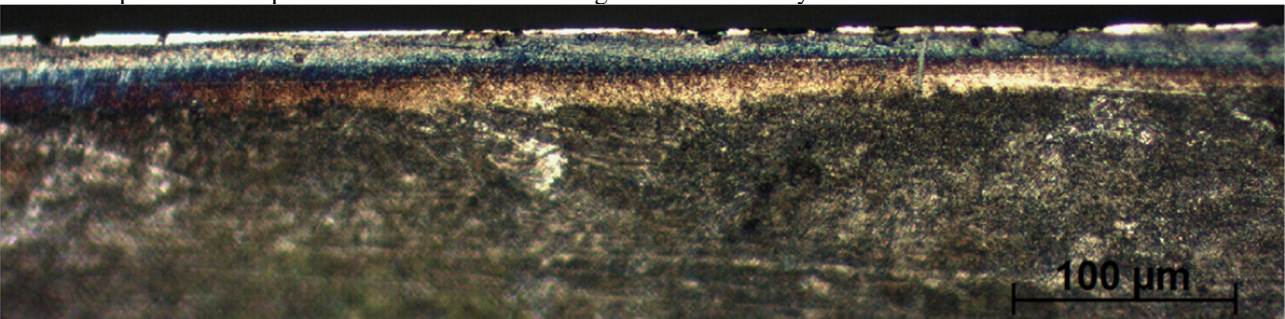
278
279 Comparing the report to the scans makes it highly likely that the initiation was in this area, and the branching of the
280 longitudinal crack occurs within 4mm of the longitudinal slice in Figure 6d, moving towards the gauge corner. Being that
281 the Y-shaped crack is closer to the field corner than the gauge corner suggests that a two point contact between the wheel
282 and the rail may have been responsible. High surface temperatures occur with lower creepage and train speed when the
283 contact patch is reduced like in a two point contact [21]. Sample 2 also contains a similar Y-shaped crack in a similar
284 region but the clarity of the two cracks is not as clear, although a higher resolution scan of that area is planned for future
285 work due to the branching of a possible transverse crack being in the same region. The L-shaped crack tracks the boundary
286 between the dark lobe of the squat and the shiny surface of the running band, it also appears to contain islands of a
287 different phase of steel, possibly martensite. This crack will be the subject of further investigations.
288 For each of the 3 samples scanned, a 3D model was created both in Avizo and in VGStudio MAX. The model shown in
289 Figure 7 was created in VGStudio MAX. The crack plane continues through the hole in the centre of the model: that
290 region was not detected by the automatic construction module, but the crack was discernible manually. The crack plane
291 also extends slightly further beyond the two green dots on the model.

Figure 7: Left) The model of the crack network in sample 1 created in VGStudio MAX showing a plane than runs parallel to the running surface to give a gauge or depth Right) a photographic reference of the surface cracks that are green in the model and yellow in the photograph

WEL varied; it appeared as both islands and long stretches, often within the same sample. An aerial view of the railhead showed long streaks of WEL and some are visible as contrast in the right image of Figure 7. Depending if the sample is cut in parallel or perpendicular to a streak probably partly explains this. The other part to consider is that WEL breaks away easily due to its brittle nature. Figure 8 shows one of the more unusual WEL found and is taken as a longitudinal slice from between the crack with a hole and the more central of the two black spots (Figure 7). It shows a bright white, fairly continuous band of WEL that seems very brittle as it has spalled in various places. This is on top of another fairly continuous WEL that has a distinct boundary with the upper layer and a more diffuse boundary with a deeper yellow patch of discrete WEL. The lower layer also has a diffuse boundary with the parent steel. It is believed that the lowest layer may have been caused by a grinding stone facet due to its discrete nature, like Figure 14, which is from outside running band. The other two layers were created by wheel slips of different magnitudes, leading to different temperatures being reached. Different temperatures will lead to differences in how much of the material reaches full austenisation as well as the penetration depth of the heat. Further investigation into these layers will be conducted in future work.

Figure 8: Three layers of WEL. The upper brighter WEL and middle duller WEL are fairly continuous for ~15mm of the 25mm sample. The upper layer is ~5 microns thick and the middle layer is ~19 microns thick. The lower, more yellow layer is a patch not much larger than the image and is ~14 microns at its thickest. A grey crack can be seen growing vertically through all 3 layers to the right of the image.

5.2. Sample 2
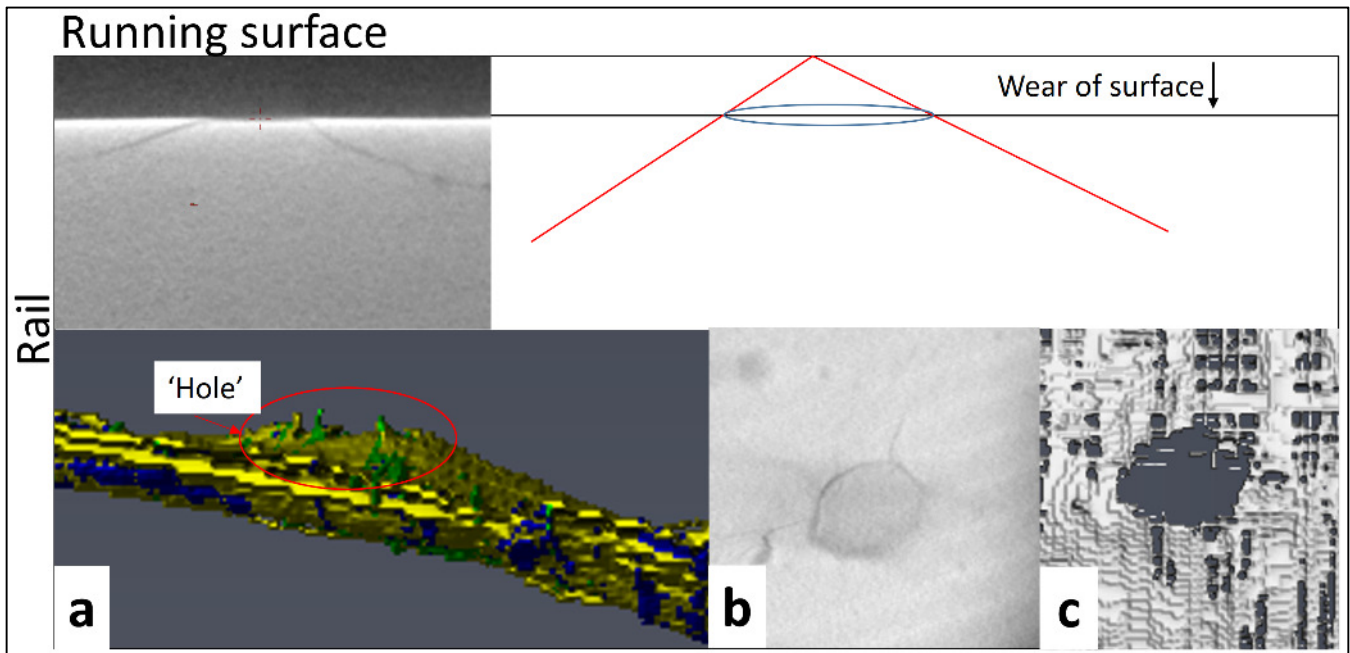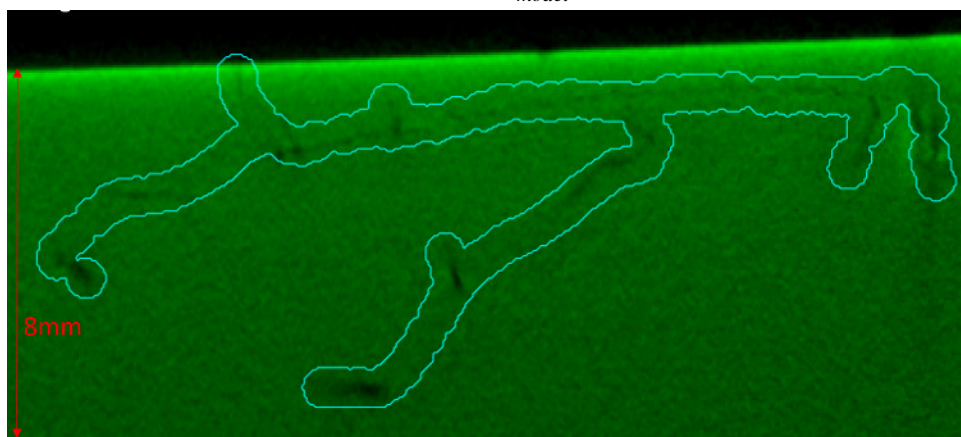
All of the samples showed the typical inverted V-shape that is expected in a longitudinal slice from a squat or stud. Sample 1 showed a branching crack propagating slightly deeper into the rail and sample 2 showed a lot more damage further along the rail from the expected inverted V-shaped crack. This damage was due to multiple branches of cracks that were turning down into the rail and continuing to branch further, as it is common for the leading crack to do. This damage was more significant than that in the other scanned samples, especially when considering the mere 11MGT of traffic experienced by sample 2.

Another detail that showed through the full construction of the models was that the 'C' and 'O' shaped cracks found in the centre of the surface of samples 2 and 4 were the location where the inverted v-shaped crack had been truncated by wear (Figure 10). Sample 1 did not have this feature but sample 3 had a surface breaking crack in the same region but of a different morphology.
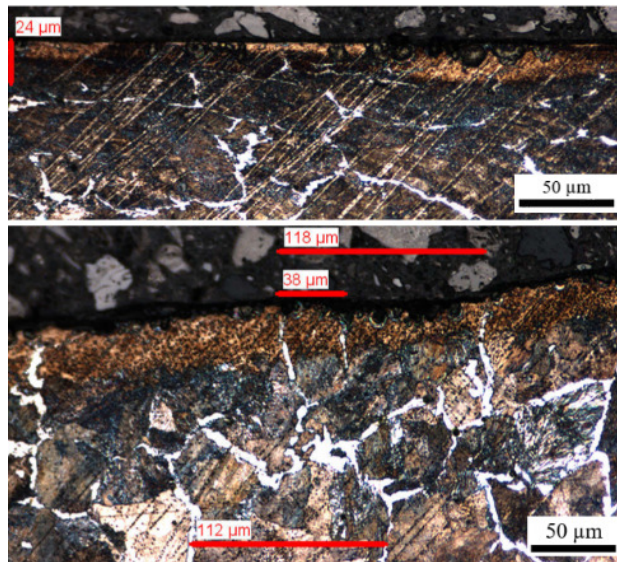

Figure 10: A diagram showing how wear truncates a pair of cracks to leave what is seen in the scan slice. Inset; a) The 'hole' from the longitudinal view as modelled in the Avizo model of sample 2, b) The original scan image of the surface of sample 2, c) The same view as (b), but of the Avizo model

Figure 9: Longitudinal orthoslice of sample 2 showing the branching cracks

Sample 2 had much more damage than expected. Figure 9 shows a longitudinal section from the scan: although the resolution of the scan is low due to the size of the sample, parts of the transverse crack can be discerned up to 8mm deep into the railhead. Cracks can be seen reaching 10mm deep in other regions of lower clarity. A higher resolution scan will be conducted on this region to clarify the structure of the deeper crack and hopefully identify the region that caused the crack to start growing into what could become a transverse defect.

WEL was found at a fairly consistent depth of 5-10 µm in some locations inside and outside the defect. There were some locations where the thickness of the WEL varied even in a very small area such as in Figure 11. Figure 10 also shows one region that was found very close to the field side of the running band, where the widened band started to narrow again. This region contained WEL with the ferrite on the grain boundary still visible as shown in the first documentation of a stud [5].

Figure 11: Above) WEL thickness varying from 1- 24 microns thick in sample 2. Below) Ferrite grain boundaries still visible within the WEL.

5.3. Sample 3

Due to the in-service break, the results obtainable from sample 3 were limited compared to the other samples. Its inclusion in the comparison was due to the known transverse defect. The undamaged lobe of the squat was still intact and it was possible to remove the upper plate using a cross-sectional cut between two of the longitudinal surface breaking cracks. This revealed a structure similar to the models of the scans along with a discrete vertical crack that broke the surface as a wide crack and penetrated slightly deeper into the rail as seen in Figure 12. The scan in Figure 12c shows the surface area before it was cut, which includes features that appear as two white cracks in the scan due to the information being lost within the crack rather than being captured by the detector. These fairly wide crack mouths are believed to be part of the remnant of the initiation site. Judging by the amount of folded over material just next to the 'white holes' there were high contact forces in this area. The material may have flowed from the ridge that often occurs between the two lobes of a squat as this ridge experiences very high contact forces. Figure 12e shows what appears to be a small void in the crack in area highlighted by the orange box in Figure 12b. This area was scanned (Figure 12f) and the morphology suggests that
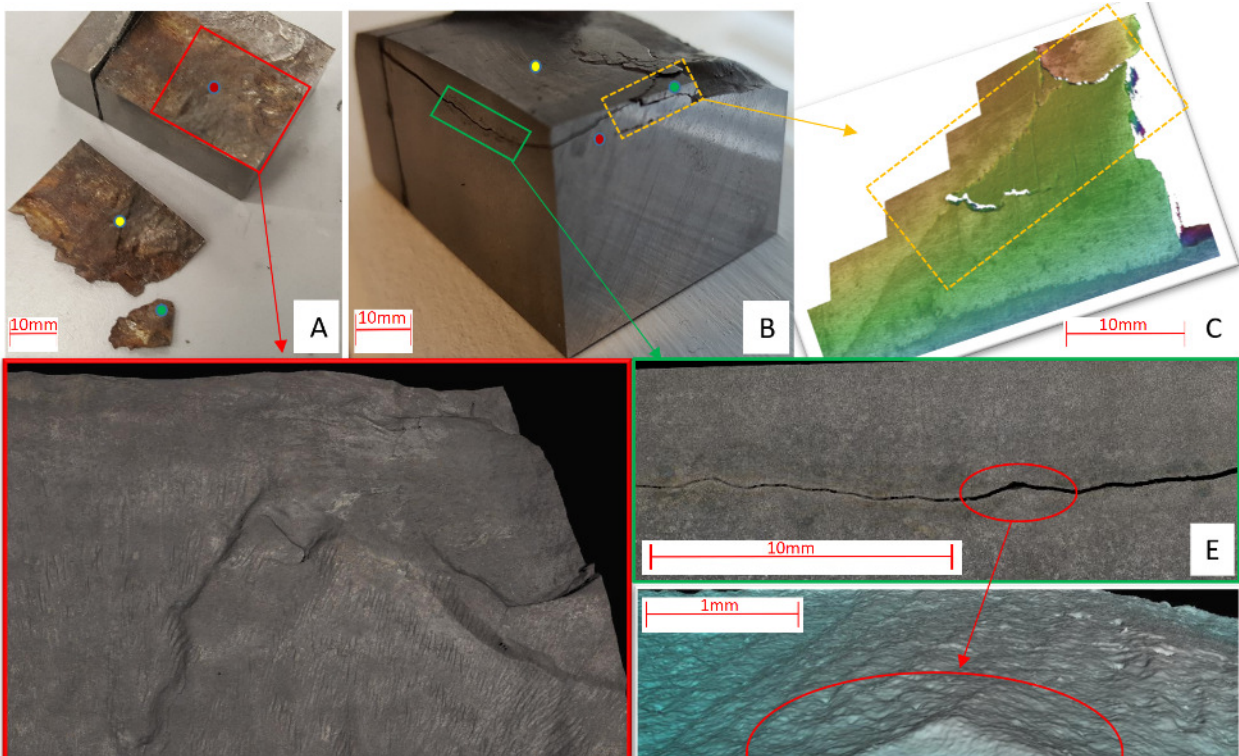

Figure 12: The fracture surface under the remaining second lobe/ spot of the squat in sample 3. A) The fracture surface immediately after removing the upper surface. B) The sample before the removal of the surface showing the two cracks propagating down into the rail from a possible initiation point. C) The 3D model of the possible initiation area taken before cutting with the orange box showing the common area D) The 3D model of the crack plane shown in A. E) An enlarged view of the green box in B showing where material has spalled away during cutting. F) A 3D model of the 'pore' in E

344 an isolated region of material ('island') caused by a branching, then converging crack. These 'islands' are found
345 throughout the crack networks of all scanned defects and cause shadows to appear as shown in Figure 17.
346 Micrographs of longitudinal slices through the region confirmed the presence of many long inclusions as well as an
347 unexpected overall microstructure (Figure 13). Inclusions were distributed throughout the steel orientated in the rolling
348 direction, the same direction as the unusual ferrite 'stripes' within the microstructure. The presence of these two unusual
349 features suggests an ingot cast steel, meaning this was probably a very old rail as many companies have moved to
350 continuous casting rather than ingot casting to produce cleaner steel. The cracks that travelled through the subsurface of
351 the rail also match the orientation of the inclusions and ferrite 'stripes' and so there is a very good chance that this unusual
352 microstructure was the cause of the shelling and failure of this rail.
353 WEL was found in thick islands in cross sectional micrographs from the gauge corner of sample 3 as shown in Figure 14.
354 This is one of three discrete but deep patches of WEL from just before the defect / widening of the band.
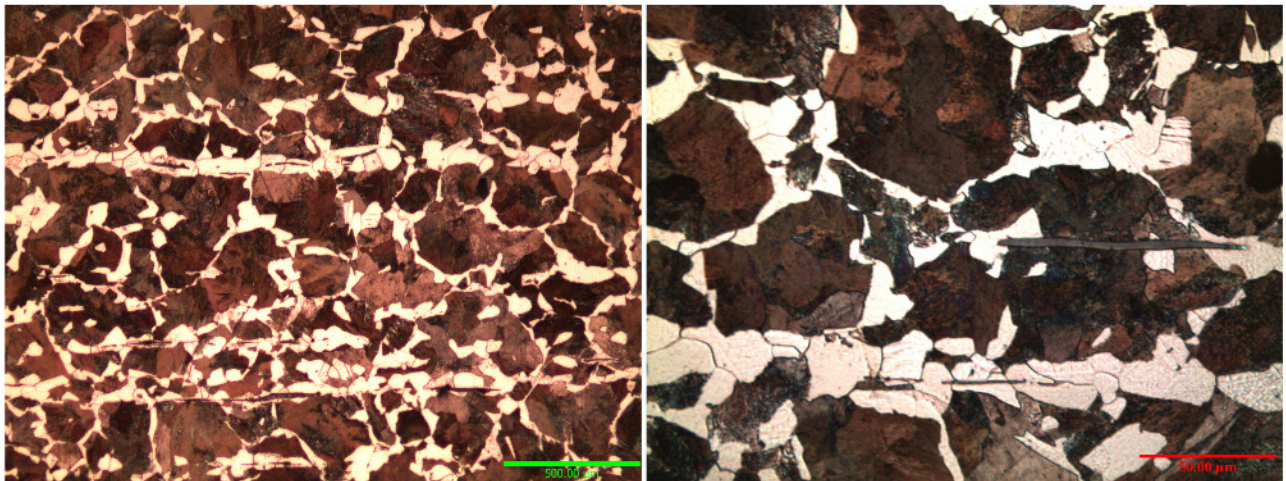355

Figure 13: *Micrographs of sample 3 at two different magnifications, showing the unusual microstructure and the inclusions found throughout the steel*
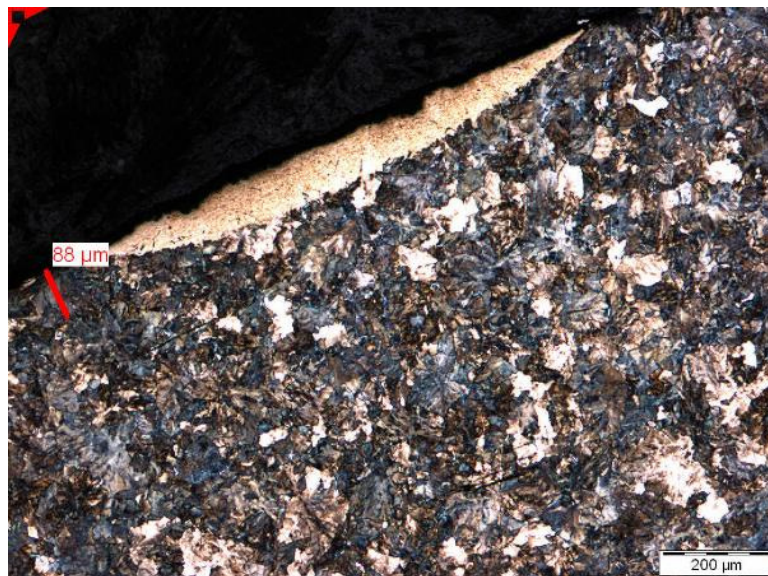

356
357 ***Figure 14:*** *Thick white etching layers on the gauge corner of sample 3*

5.4. Sample 4

359 Sample 4 had much less damage than expected, based on the results of the ultrasound tests. The ultrasound gave reason
360 to expect a weld defect as well as the surface defect. However, there was no sign of a weld defect in the upper 26mm of
361 the head and the welds heat affected zone (HAZ) did not seem to have much influence on the crack planes overall
362 morphology. The crack plane was extensive but travelled at a fairly constant angle with few deviations other than the
363 'hole' (Figure 10a) where it surfaces into the C-shaped hole, which is on the boundary between the weld and the rail. No
364 unusual hardness variation was noticed across the HAZ.
365 The initiation is believed to have been due to the spheres/ bubbles found above and below the proposed initiation site
366 (Figure 15). Small cracks were seen travelling between these spheres in the region directly below the cracks. Sample 4
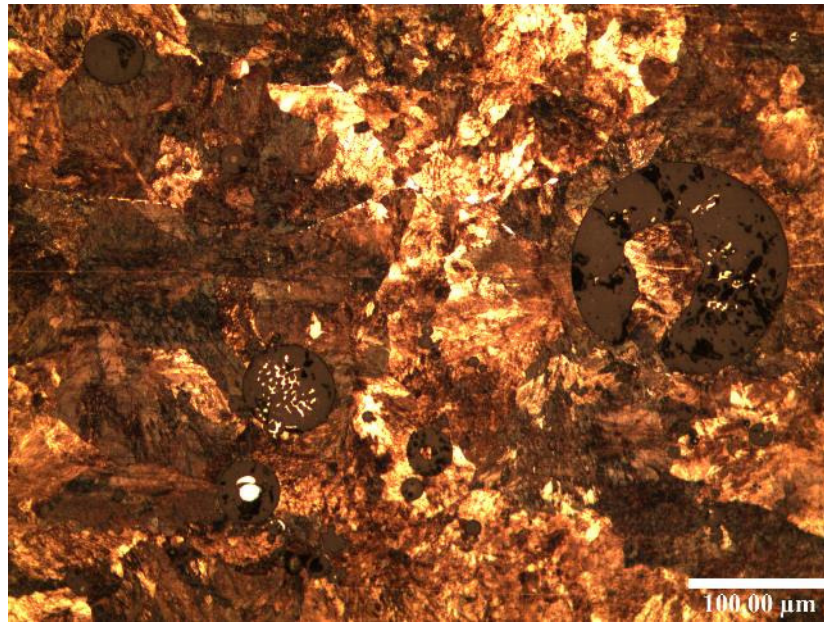367 was the most benign of all of the samples as it was the only crack network that did not branch.

Figure 15: *Spheres or bubbles found in the microstructure of the weld edge of sample 4 from within the green box in Figure 18. Probably either gas trapped in the melt or slag from the welding process*
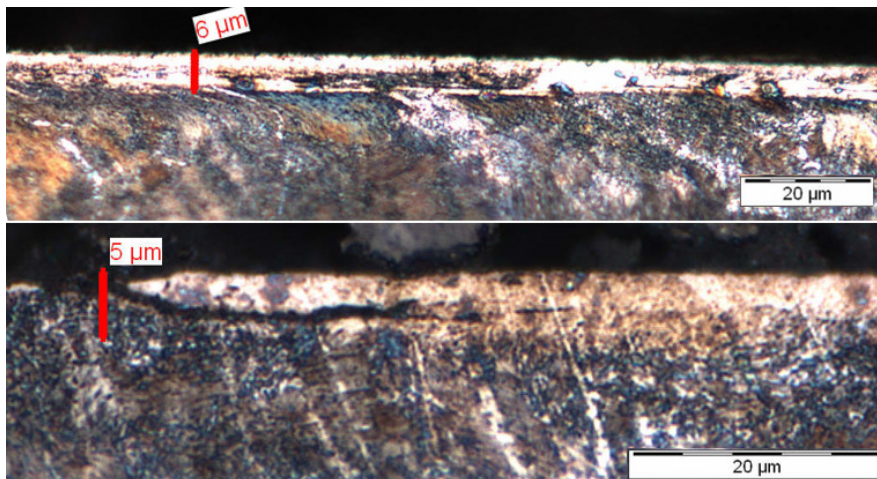
368

369
370

Figure 16: *Above) WEL from within the defect. Below) WEL outside the defect*

371   WEL was also found at a very consistent depth of 5-7 microns inside and outside the defect (Figure 16). The visible
372   grinding marks on the surface make it probable that this WEL is due to the grinding process. The WEL inside the defect
373   had a more distinct boundary with the parent material compared to outside the defect.
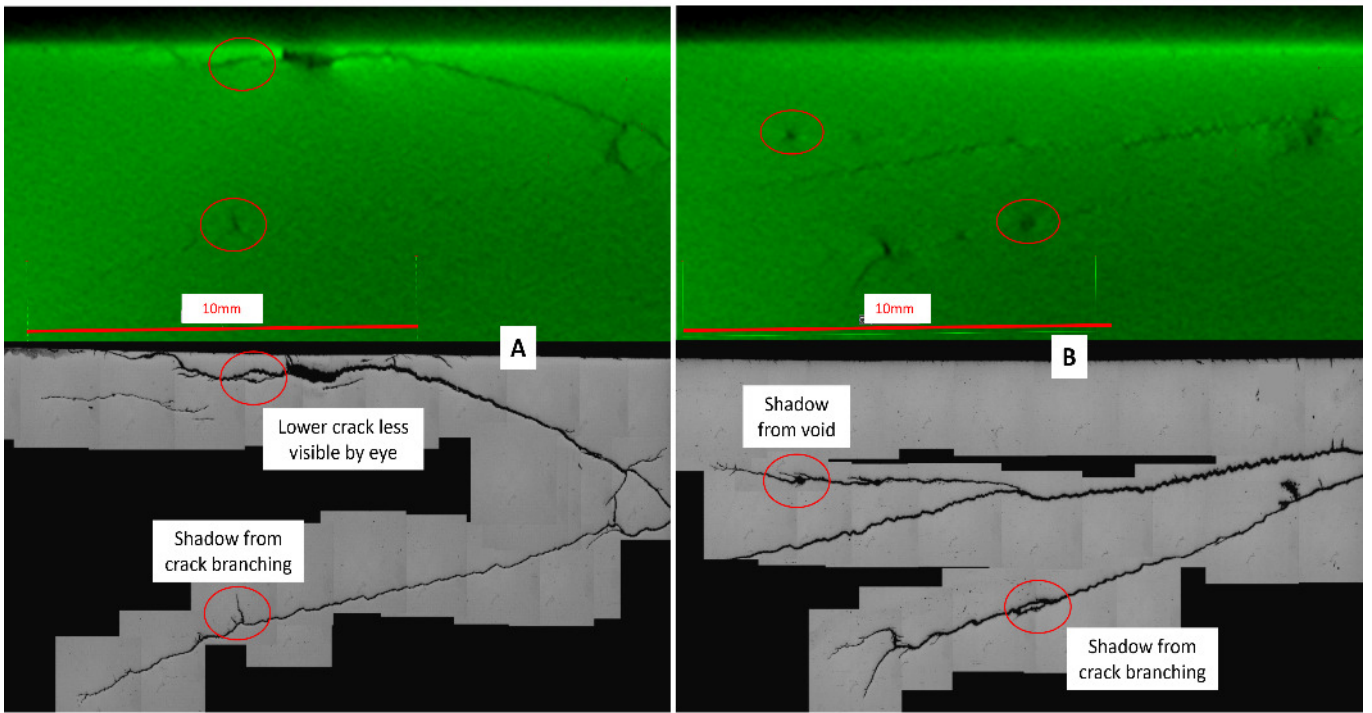
374
375   ***5.5. Scan verification***
376   In sample 1, an orthoslice of interest was one that showed a crack branch down from what appeared to be a small void on
377   the surface, which was visible from the surface scans. The crack then displayed interesting behaviour by branching in a
378   circular shape as though propagating around something that it could not penetrate. There were also small shadows on the
379   scans, which were investigated to see how real they were. Figure 17 shows the two comparisons of the scan slices
380   mentioned and their accompanying micrograph. The upper red circle shows a region where the finer crack does not show
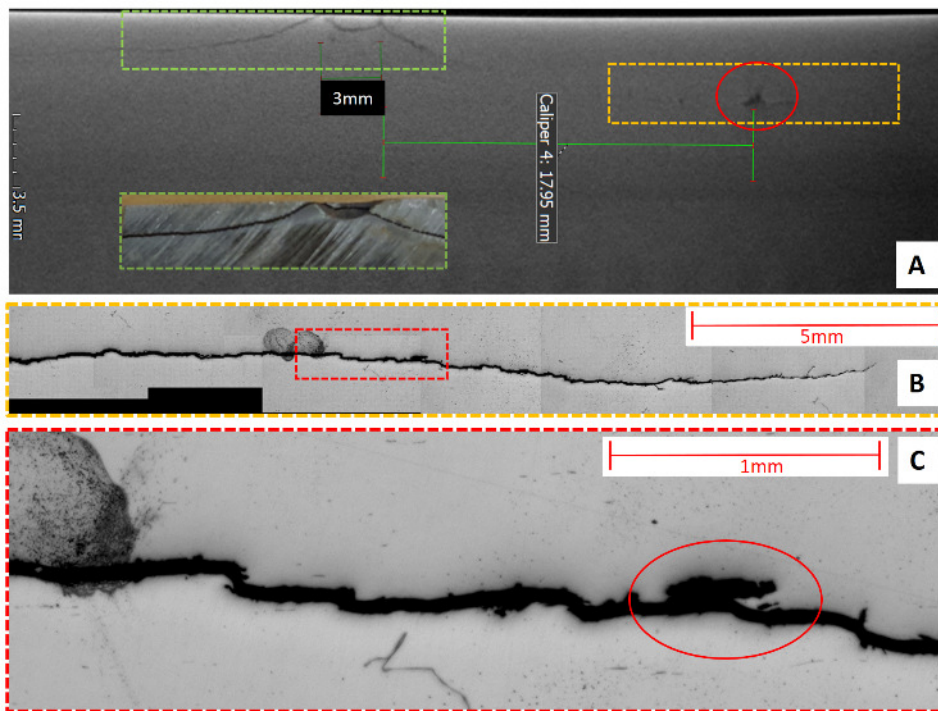381   but the larger crack does and the lower circle shows how a branching crack can create a shadow.
382   Sample 4 also showed a shadow near the surface breaking feature in the centre of the rail and the verification of that scan
383   is shown in Figure 18. Figure 18 shows; a shadow found on the crack within the CT scan, the cause of that shadow and
384   verification of the structure shown in the green box, which is responsible for the C shaped crack that breaks the surface
385   of the running band. It also shows a zoomed image of the area that caused the shadow to appear: a small void. These voids
386   are believed to develop from the small 'islands' like the one labelled "shadow from crack branching" in Figure 17b due
387   to rubbing of the crack surfaces wearing away and eventually breaking up the 'island'. The broken debris from the island
388   could cause variations in the x-ray interaction that, when reconstructed into a CT volume, would appear like a void. The
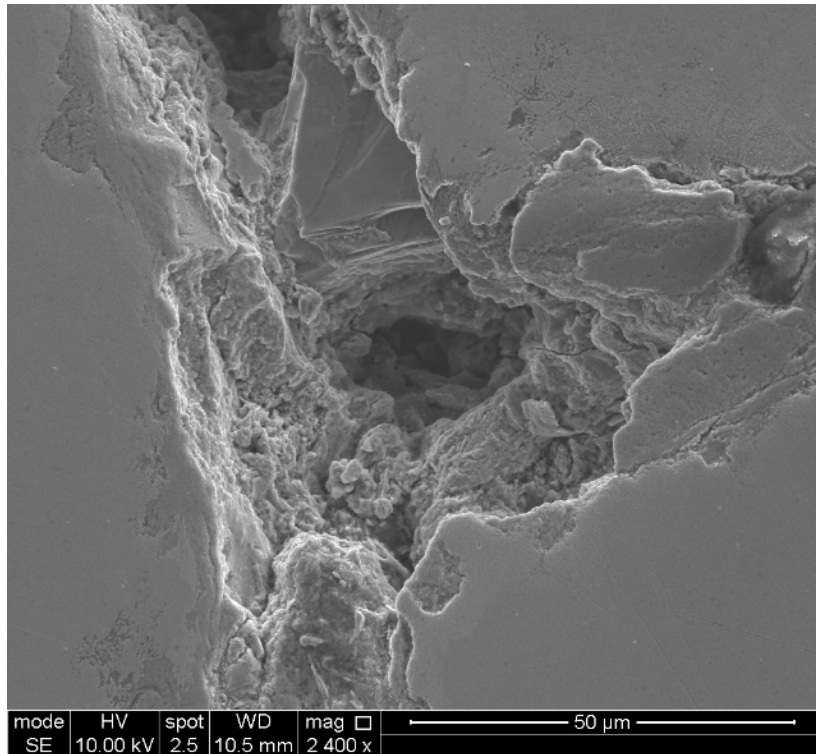389   broken debris would then be washed out during sample preparation.

390

Figure 17: *Comparison of longitudinal CT scan orthoslice to longitudinal section in sample 2 a) The surface void visible from the surface scans with a shadow and its cause highlighted b) Branching that shows shadows in the scan and the same cause as (a) in the micrograph.*

391

Figure 18: *Longitudinal slice through the c-shaped crack in the centre of the surface of sample 4. a) CT scan orthoslice showing the surface breaking crack highlighted in the green box with a photo of the sectioned sample inset in the lower green box b) An unetched micrograph of the area highlighted in the orange box c) An expanded view of B, with a red circle showing the cause of the shadow in the CT scan orthoslice (a).*
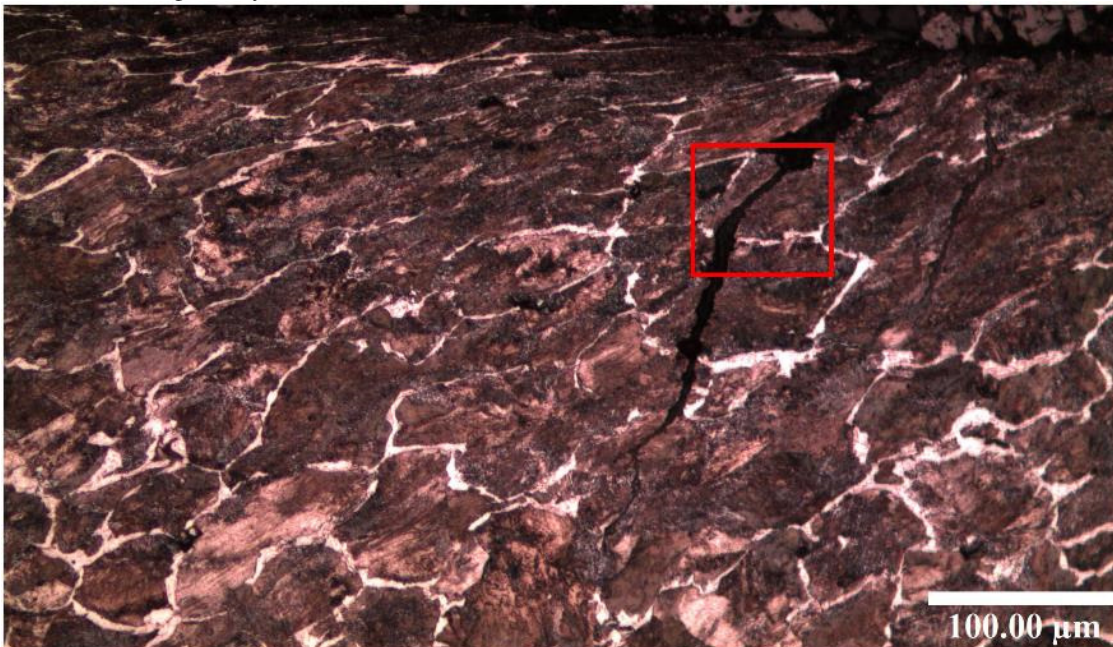
392   These voids are possible branching points for the crack as features like these voids have been noticed at the junction of
393   crack boundaries as shown in the SEM image in Figure 19. The void is from the circular crack in Figure 17a, and may
394   have been why a crack branched down from the main crack, or may be due to fretting after the crack branched. It is hard
395   to be sure due to so much damage and corrosion. Sample preparation will also cause some material loss from the area
396   shown.

Figure 19: *SEM image of a junction where a crack branched off deeper into the rail.*

5.6. Microstructural sensitivity

Figure 20 shows an optical micrograph of sample 3 with a surface breaking crack. The crack travels fairly vertically through the material rather than at an acute angle to the surface as is usually expected from RCF cracks. This is seen in thermally damaged steel [22]. The interesting behaviour regarding the crack path is that unlike squats, which typically follow inter-granular ferrite, this crack seems to cut across the grain as documented by Grassie et al. [5]. However, unlike the studs investigated by Grassie et al. this behaviour also occurs within 450 microns from the surface as well as below.
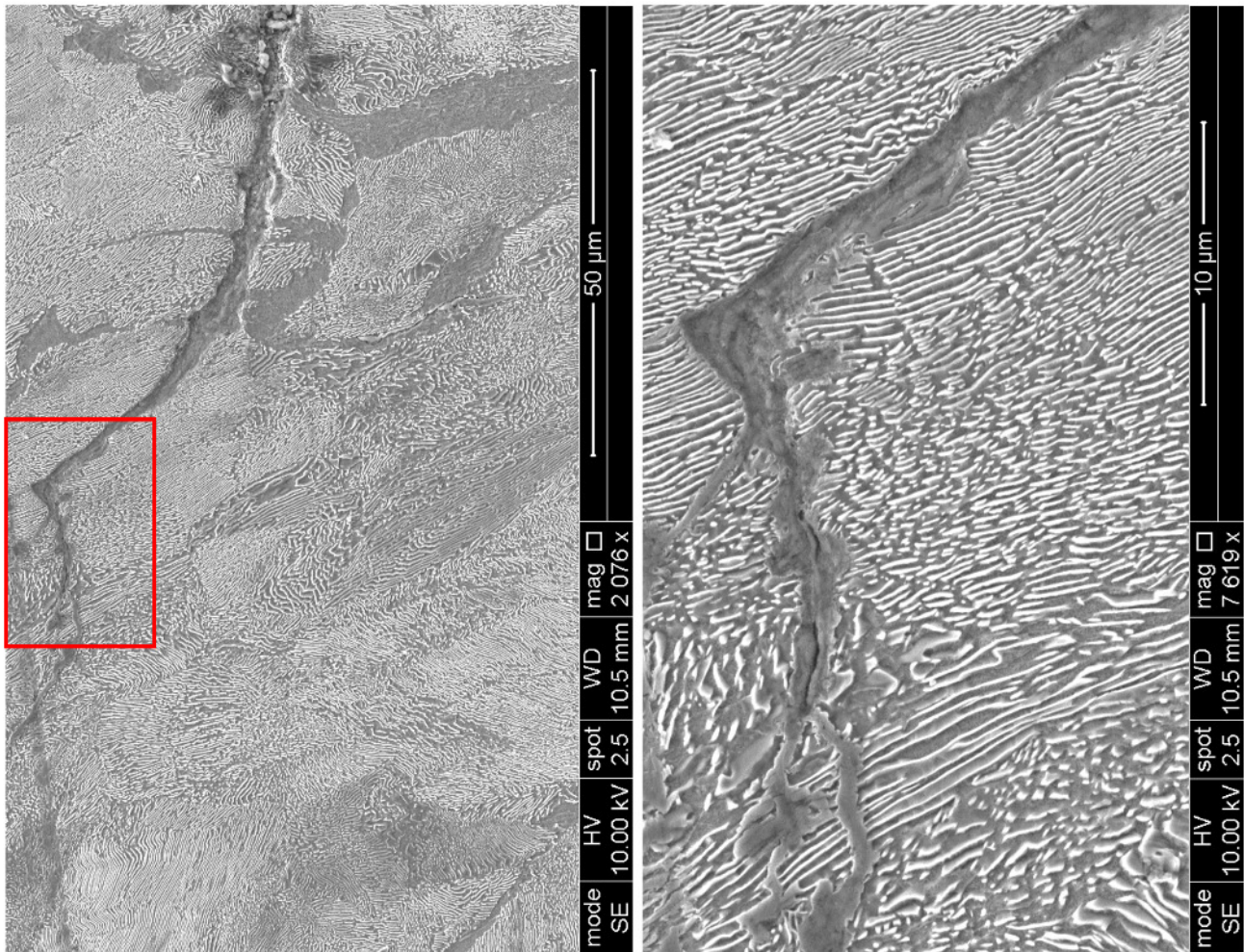

Figure 20: *Optical micrograph of sample 2 showing a surface crack with apparent non-sensitivity to microstructure. The red box shows where SEM images were taken from (shown in Figure 21)*

It should be noted that although the crack seems to ignore the grain in this orthoslice of the rail, it may follow the microstructure more carefully closer to its origin and lose that sensitivity as it propagates out in 3D.

The SEM was used to look closer at the crack in Figure 20 to see if it is completely insensitive to the grain structure.

As seen in Figure 21, the cracks travel between lamellae plates a majority of the time but not always. They seem to be able to change direction when the plates become small and more spheroidal. There are places where this is not true such

as the bottom of the right SEM image where the cracks cut straight through plates. This could be because the crack was well developed in orientation to the lamellae of a neighbouring grain and so continued in that orientation as it widened. This would mean that the crack did not initially grow within this slice following these grain orientations. Looking at the CT scan data in 3D the crack plane grows down into the rail and diagonally across the rail as it propagates longitudinally and laterally at the same time. This means that the initial crack path cannot be viewed in its entirety, with regards to the microstructure, within one micrograph. Many thin slices will need to be taken around the possible initiation site to investigate the relationship between microstructure and the crack path to its full extent. This will be part of further work.

Figure 21: Left) SEM image of the box from Figure 20 showing that the crack still prefers to travel between the lamellae plates of the pearlite when cutting across grains. Right) magnified view of the box in the left image.

6. Discussion

Although the four defects are from different countries and track environments, they all share a longitudinal crack along the edge of the running band. This shows how heavily developed they are as this is where the crack plane finally surfaces. This surfacing was probably recent in sample 2 as the crack is still rough. The kink in the longitudinal crack of sample 2 is because there are two defects very close together that merge and break the field side of the running band as two separate, but similarly located crack.

Both metro samples (1 and 2) had a Y-shaped crack that was also found in the literature [20]. This Y-crack is believed to be the first to develop of the various cracks found in samples 1 and 2 and is on the field corner half of the railhead rather than towards the gauge corner. The cooling that occurs after excessive wheel slip is higher outside the contact patch and considering the damage from thermal input is caused by tensile stress during cooling [22], this could explain why early cracks such as the Y-shaped crack occur easier on the edges of the contact patch. The presence of two unconnected cracks under the Y-shaped crack brings in the possibility of two initiations, one subsurface and one close to or on the surface. It is likely that one appeared first then the other as a result, as the leading-trailing crack theory in the literature mentions.

Samples 2 and 4 have a 'hole' in the running band where the conical crack has been truncated as the tip is worn down. This hole had a loose piece of material in the centre that was lost during cutting, so it was beneficial to have preserved this information in the scans. The next few paragraphs will discuss each sample in turn;

Sample 1 was initially believed to be a stud because of its fairly smooth surface and the likelihood of a bad wheel slip event being from an incline. However, the presence of lipping on the edge of the rail (i.e. plastic flow) brought this into question. Sample 1 is lacking the 'hole' that was noted in sample 2 and 4 despite having significantly more surface damage than any of the other three samples (or the reported squat that it was compared to in section 6.1). The lack of plastic flow on the surface, smoothness in both directions and the islands of WEL found make it highly likely that this is a stud and that the lipping was not due to the defect.

Sample 2 is believed to be a stud, primarily because of its very low MGT, smooth surface and lack of plastic deformation. Checks for lubricant penetration were not conducted on any of the samples as they were contaminated by cutting fluids whilst trying to expose the cracks. There were pits above the most damaged region with two pits being connected by a surface crack. Investigations into more samples that have this feature would be very beneficial as it may explain why the defect was so well developed considering there was so little traffic on that rail. This is based on the principle that a rough surface causes much higher subsurface stresses. This will be a topic of future work.

The wider crack in the V on sample 3 is where the cracks meet near the surface making this a likely initiation point due to ductility exhaustion. Sample 3 was had long inclusions running parallel to the cracks that caused the failure, so they are believed to have been heavily responsible. However, the whole rail probably had these inclusions so there must have been an event that initiated it, but not enough is known about the rail or its location. The presence of so many inclusions suggest that the steel was from ingot casting rather than the cleaner method of continuous casting.

Contamination in the very upper part of the weld is believed to be responsible for the initiation of the defect in sample 4. The contamination consists of just a few spheres/ bubbles of unknown composition (probably gas or slag) very close to the surface. Cracks were observed between these spheres/ bubbles.
There is only one region where there are variations in the cracks, the only other features are simple and linear cracks that propagate just under the surface as expected. The weld does not seem to affect the crack structure and the only noticeable difference is that the crack structure is longer in the longitudinal direction: this could be due to more MGTs, not necessarily the higher speeds experienced. Overall sample 4 had less branching than the metro or mixed traffic samples, possibly due to modern track construction and less traffic variation/ better profile matching between the wheel and rail.

Table 3 summarises the more comparable points made in the discussion;

Feature	Defect 1	Defect 2	Defect 3	Defect 4
Surface cracks	Longitudinal. V-shape. Y-shape crack.	Longitudinal. V-shape. Y-shape crack. 'Hole' from truncated cracks.	Longitudinal. Probable V-shape.	Longitudinal. Hole' from truncated cracks.
Undesirable microstructural content			Large inclusions	Weld contaminants
Other surface features	Snakeskin that left pits upon spalling	Pitting and obvious grinding marks.	Folded material. Lost material due to transverse fracture.	Weld zone and obvious grinding marks. '
WEL	Triple layer found at 5- 19 microns thick. ~5 microns more typical of other slices through defect.	Varying thickness but up to 24 microns thick.	Discrete patch 88 microns thick	5-7 microns thick

Table 3: Summary of comparisons between defects

The scans allow comparison of samples even if the same cuts were not made in sample preparation. Access to the sample that sample 1 is compared to is unavailable but being able to move through a volume allowed the same specific feature to be found, even though it was only ~1mm wide. A library of μ-CT scanned defects would allow a more comprehensive comparison of different defects and would aid in categorising them. The details in the scan were verified by comparison to micrographs of the sample after micro-preparation. Figure 17 and Figure 18 show that the shadow highlighted by the red circle is real and the faint traces of the upper crack are real too. The uppermost crack was not obviously a crack like the lower two were so the scan did not depict all of the cracks with the same clarity. This is due to the size of the sample scanned, i.e. smaller samples are easier to image clearly.

Focus on the crack path through the microstructure would aid in adjusting the microstructure to resist crack growth. To fully understand why the crack path takes the route it does, it needs to be traced in detail from where the initiation begins through to a depth where the crack shows little or no sensitivity to microstructure at all. The need for this work to be carried out requires a good idea of the initiation site and a defect that is not too well developed as to have lost too much information due to the wear and deformation of the surface.

7. Conclusions

Each defect is different to each other, both in cause and morphology. It is difficult to be sure how much the traffic type influences the differences seen as track information was scarce with most of the samples. Some common features amongst metro samples were notable though. Studs from the metro networks in France and the UK seem to share a Y-shaped crack feature: containing subsurface cracks that seem to have developed independently rather than branching from a single point. This region is possibly part of the early initiation as the sample referenced in section 5.1 only contained this crack and some 'snakeskin'. This crack being located on the very edge of the contact patch suggests possible initiation by a two point contact/ hollow wheel.

Surface breaking 'holes' in sample 2 and 4 are a feature for two of the studs and are truncated inverted V-shaped structures typically found in both squats and studs.

Based on the four samples compared, studs may be far more common than initially expected, especially on metro and high speed lines. The track operators initially identified all the four samples as squats.

The classification and probable cause of the four samples are shown in Table 4:

Sample	Identity	Cause
1	Stud	High contact stress
2	Stud	High contact stress
3	Squat	Inclusions
4	Potentially squat or stud	Contaminated weld

Table 4: Defect identity of samples examined

The cause listed in Table 4 are in combination with wheel slip for the stud defects. The wheel slip is the cause of the thermal damage needed to initiate the crack structure. There are notable deep grinding marks over the defect in sample 2 but their role, if any, in the initiation needs to be investigated further.

The studs seen in this work share most of the features originally documented by Grassie et al. [5], but have a few differences to the studs such as cracks crossing grains close to the surface as well as deeper into the rail. There also seems to be less WEL, especially regarding depth. This could be that these studs experienced a different history of temperature change, perhaps due to a different contact patch or other tribological factors. Both previously documented studs and the studs seen here both show signs of thermal influence. Determined in this work due to grain refinement in some areas, an overall lack of plastic flow and the presence of fairly vertical cracks that break the surface. Vertical cracks are often seen through thick WEL but none was seen in the presence of these cracks, though that does not guarantee that it was never there.

This is just a tiny number of defects examined compared to how many occur, but there are differences between them despite them appearing to be the same initially. The traffic experienced is highly likely to be a factor considering the load differences between light rail/metro and heavy haul/ freight. The surprise with this work was that one of the lightest axle loads produced a complex crack network, possibly due to a much lower natural wear rate. It did not grow anywhere near as deeply as sample 3 but the ages of the two samples cannot be compared. Sample 3 is likely much older considering it seems to have been ingot cast.

There would be great benefit in creating more CT volumes of squat and stud samples at various stages of development, allowing detailed comparison of defects and aid in searches for specific features. It cannot be determined from this work if a CT scan can discern between a squat and a stud as all 3 samples that were scanned are believed to be studs. The studs were noted as two being from metro and one from high speed with the squat being from a mixed traffic environment. It should be noted that the squat is believed to have failed due to material as well as the service environment, so it is difficult to conclude accurately where squats appear compared to studs just from these four samples.

8. Further work

Further research will be conducted on more regions within all four samples, particularly the metro samples, looking at microstructural details such as plastic flow, WEL and crack paths. The cause of the shadows in the scans have been seen to be the branching of cracks either as junctions, 'islands', voids (broken up islands), but these features will be investigated further. Hardness mapping will also be used to look for variation in hardness from the thermal expansion and contraction

experienced by the surface region of the railhead, to support their identity as studs. Further μ-CT scans will be conducted on sample 2 at a higher resolution to investigate the transverse branching crack origin. Verification of the early work presented on microstructural sensitivity to crack growth paths will be conducted as detailed in the discussion. Mechanical tests will be conducted using small scale rigs to simulate the thermal damage observed in some of the samples presented. Grinding marks have been noted as being present on multiple samples so more work will be conducted into the effects that surface imperfections such as grinding marks and pits have on squat type defects. Work will also continue to improve the accuracy of the models of crack networks produced from the scans, to be presented in future work.

References

[1] M. Molodova, Z. Li, A. Nunez, and R. Dollevoet, "Automatic Detection of Squats in Railway Infrastructure," *IEEE Traansactions Intell. Transp. Syst.*, vol. 15, no. 1, pp. 1980–1990, 2014.

[2] Z. Li, R. Dollevoet, M. Molodova, and X. Zhao, "Differential wear and plastic deformation as causes of squat at track local stiffness change combined with other track," no. 789271101, 2008.

[3] International Union of Railways, "INNOTRACK concluding technical report," Paris, France, 2010.

[4] Network Rail, "Rail Head Squats," 2015. [Online]. Available: https://cdn.networkrail.co.uk/wp-content/uploads/2017/03/Challenge-Statement-Track-Plain-line-rail-head-squats.pdf. [Accessed: 13-Jun-2018].

[5] S. L. Grassie, D. I. Fletcher, E. A. Gallardo Hernandez, and P. Summers, "Studs: a squat-type defect in rails," *Proc. Inst. Mech. Eng. Part F J. Rail Rapid Transit*, vol. 226, no. 3, pp. 243–256, 2011.

[6] D. I. Fletcher, P. Hyde, and A. Kapoor, "Investigating fluid penetration of rolling contact fatigue cracks in rails using a newly developed full-scale test facility," *Proc. Inst. Mech. Eng. Part F J. Rail Rapid Transit*, vol. 221, pp. 35–44, 2007.

[7] D. I. Fletcher and S. H. Sanusi, "the Potential for Supressing Rail Defect Growth Through Tailoring Rail Thermo-Mechanical Properties," in *10th International Conference on Contact Mechanics and Wear of Rail/Wheel System*, 2015.

[8] M. Kerr, A. Wilson, and S. Marich, "The epidemiology of squats and related rail defects," *CORE 2008 Conf. Railw. Eng. rail- the-core Integr. Transp.*, no. September, pp. 83–96, 2008.

[9] ARTC, "Rail Defects Handbook Some Rail Defects , their Characteristics , Causes and Control RC 2400," no. March, 2006.

[10] E. N. Landis and D. T. Keane, "X-ray microtomography," *Mater. Charact.*, vol. 61, no. 12, pp. 1305–1316, 2010.

[11] M. Naeimi *et al.*, "Reconstruction of the rolling contact fatigue cracks in rails using X-ray computed tomography," *NDT E Int.*, vol. 92, no. April, pp. 199–212, 2017.

[12] NSW Transport RailCorp, "Rail Defects Handbook: TMC 226," pp. 1–83, 2012.

[13] X. Deng, Z. Qian, Z. Li, and R. Dollevoet, "Investigation of the formation of corrugation-induced rail squats based on extensive field monitoring," *Int. J. Fatigue*, vol. 112, no. February, pp. 94–105, 2018.

[14] F. J. Franklin, I. Widiyarta, and A. Kapoor, "Computer simulation of wear and rolling contact fatigue," *Wear*, vol. 250, no. 251, pp. 949–955, 2001.

[15] D. Scott, D. I. Fletcher, and B. J. Cardwell, "Simulation Study of Thermally Initiated Rail Defects," *Proc. Inst. Mech. Eng. Part F J. Rail Rapid Transit*, vol. 228, no. 2, pp. 113–127, 2012.

[16] N. Gao, R. S. Dwyer-Joyce, and D. G. G. Grieve, "Disc machine testing to assess the life of surface-damaged railway track," *Proc. Inst. Mech. Eng. Part F-Journal Rail Rapid Transit*, vol. 215, no. 4, pp. 261–275, 2001.

[17] Z. Li, X. Zhao, C. Esveld, R. Dollevoet, and M. Molodova, "An investigation into the causes of squats-Correlation analysis and numerical modeling," *Wear*, vol. 265, no. 9–10, pp. 1349–1355, 2008.

[18] A. Kapoor, F. J. Franklin, S. K. Wong, and M. Ishida, "Surface roughness and plastic flow in rail wheel contact," vol. 253, pp. 257–264, 2002.

[19] J. F. Barrett and N. Keat, "Artifacts in CT: Recognition and Avoidance," *RadioGraphics*, vol. 24, no. 6, pp. 1679–1691, 2004.

[20] H. M. Smith, "An examination of squat defects in a 60E1 R260 rail removed from the Bussy Saint Georges test site in the Paris suburbs (RER line)," Rotherham, UK, 2011.

[21] C. Bernsteiner, G. Muller, A. Meierhofer, K. Six, D. Kunstner, and P. Dietmaier, "Development of white etching layers on rails: simulations and experiments," *Wear*, vol. 366–367, pp. 116–122, 2016.

[22] J. H. You, "Damage and fatigue crack growth of Eurofer steel first wall mock-up under cyclic heat flux loads. Part 2: Finite element analysis of damage evolution," *Fusion Eng. Des.*, vol. 89, no. 4, pp. 294–301, 2014.